JOURNAL OF THE ROYAL SOCIETY Interface

Three-dimensional identification of stem cells by computational holographic imaging

Inkyu Moon and Bahram Javidi

J. R. Soc. Interface 2007 **4**, 305-313
doi: 10.1098/rsif.2006.0175

JOURNAL OF THE ROYAL SOCIETY Interface

J. R. Soc. Interface (2007) **4**, 305–313
doi:10.1098/rsif.2006.0175
Published online 21 November 2006

Three-dimensional identification of stem cells by computational holographic imaging

Inkyu Moon and Bahram Javidi*

Department of Electrical and Computer Engineering, U-2157, University of Connecticut, Storrs, CT 06269-2157, USA

We present an optical imaging system and mathematical algorithms for three-dimensional sensing and identification of stem cells. Data acquisition of stem cells is based on holographic microscopy in the Fresnel domain by illuminating the cells with a laser. In this technique, the holograms of stem cells are optically recorded with an image sensor array interfaced with a computer and three-dimensional images of the stem cells are reconstructed from the Gabor-filtered digital holograms. The Gabor wavelet transformation for feature extraction of the digital hologram is performed to improve the process of identification. The inverse Fresnel transformation of the Gabor-filtered digital hologram is performed to reconstruct the multi-scale three-dimensional images of the stem cells at different depths along the longitudinal direction. For recognition and classification of stem cells, a statistical approach using an empirical cumulative density function is introduced. The experiments indicate that the proposed system can be potentially useful for recognizing and classifying stem cells. To the best of our knowledge, this is the first report on using three-dimensional holographic microscopy for automated identification of stem cells.

Keywords: digital holography; statistical pattern recognition; three-dimensional image processing; Gabor wavelets

1. INTRODUCTION

Optical coherent imaging systems using digital holography (Goodman & Lawrence 1967; Yatagai *et al.* 1987; Osten *et al.* 2002; Kreis 2005; Nomura *et al.* 2006; Shortt *et al.* 2006) have been investigated for three-dimensional visualization and recognition of objects (Javidi & Tajahuerce 2000; Frauel & Javidi 2001; Tajahuerce *et al.* 2001; Javidi 2002; Javidi & Kim 2005). Digital holographic-based three-dimensional microscopy has been applied to the three-dimensional sensing, visualization and recognition of micro-organisms (Javidi *et al.* 2005; Moon & Javidi 2005, in press). Holographic microscopy can automatically produce multiple focused images of biological micro-organisms from only one digital hologram without any mechanical scanning, which is necessary in conventional microscopy. In addition, the depth information of the biological micro-organisms can be obtained by analysing the coherent interference pattern. Single-exposure online (SEOL) digital holography (Javidi & Kim 2005) enables one to three-dimensionally sense, monitor and recognize the moving, growing and reproducing biological cells. SEOL digital holographic microscopy allows the computational reconstruction of three-dimensional images of growing and dividing biological cells from just one digital hologram.

Stem cells have many potential applications in new medical treatments (National Institutes of Health 2004; Shostak 2006). Recently, scientists have studied stem cells to find effective treatments of many severe human diseases, such as diabetes, heart disease and Parkinson's disease. Therefore, automated stem cell monitoring, identification and classification are essential in developing such medical treatments. However, cell identification and classification is currently performed by traditional techniques, including biomolecular processing, which are not real time and may be time-consuming.

In this paper, we investigate three-dimensional sensing and identification of stem cells using coherent optical imaging based on digital holographic microscopy and statistical pattern classification. The Fresnel diffraction patterns of stem cells are optically recorded by SEOL holographic microscopy interfaced with a computer. In order to extract specific features from the diffraction patterns of stem cells, we computationally apply Gabor wavelet filtering (Gabor 1946; Daugman 1985; Lades *et al.* 1993; Lee 1996; Oppenheim *et al.* 1996) to the recorded diffraction patterns. Next, the multi-scale and multi-resolution complex-valued magnitude three-dimensional images of the stem cells are numerically reconstructed from the Gabor-filtered SEOL digital hologram. For three-dimensional classification, the empirical cumulative density function (ECDF; Hollander & Wolfe 1999) is calculated from the sample segment features, which are obtained from the multi-scale and multi-resolution three-dimensional

*Author for correspondence (bahram@engr.uconn.edu).

Received 9 September 2006
Accepted 20 October 2006

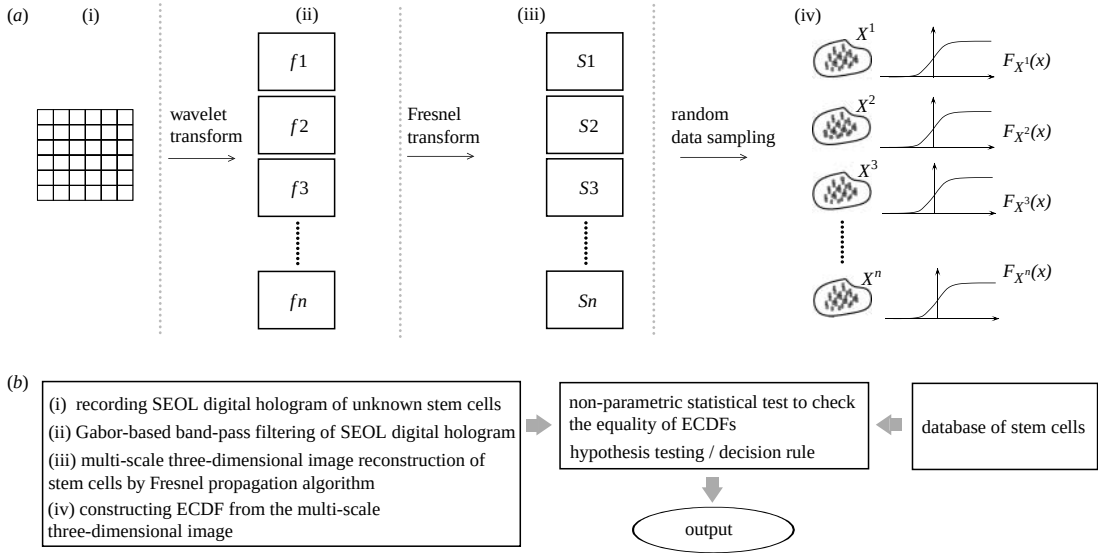

Figure 1. Block diagram for the three-dimensional recognition of stem cells using a non-parametric statistical approach. (i) Digital hologram of stem cells. (ii) Multi-scale/resolution digital holograms using the Gabor wavelet method. (iii) Three-dimensional images reconstructed from the multi-scale/resolution digital holograms. (iv) Construction of the empirical cumulative distribution function from the three-dimensional images.

images. Statistical estimation and statistical hypothesis testing are performed to compare various cells under investigation.

Figure 1 shows the framework and design procedure for three-dimensional sensing and recognition based on SEOL holographic microscopy. The following sections describe various stages of the proposed approach for three-dimensional sensing and recognition of stem cells by the use of optical coherent imaging based on digital holographic microscopy. In §2, we briefly describe the concept of SEOL digital holographic microscopy. The design procedure for three-dimensional sensing and recognition of stem cells is described in §3. The statistical analysis and statistical hypothesis testing are explained in §4. Preliminary experimental results using SEOL holographic microscopy are presented in §5 and we conclude in §6.

2. PRINCIPLES OF SINGLE-EXPOSURE ONLINE DIGITAL HOLOGRAPHY

A SEOL digital hologram of biological cells in the Fresnel domain is recorded with an image sensor array using a reference wave, as shown in figure 2. An argon laser with centre wavelength of 514.5 nm is used as a light source for spatial and temporal coherent imaging. The coherent light source illuminates the stem cell and then it starts to diffract. The microscope objective magnifies the Fresnel diffracted pattern of the stem cell and images it to the hologram plane. The image sensor array captures the interference of the reference wave and the diffracted wavefronts from the stem cell, resulting in an intensity pattern that contains both the magnitude and phase information of the stem cell.

The system requires only a single-exposure recording to obtain the Fresnel diffraction pattern of a stem cell. Therefore, SEOL digital holographic microscopy can be suitable for recognizing and identifying growing and dividing stem cells. In addition, the system is robust to external noise factors, such as environmental fluctuation and vibration, since multiple exposures are not required, as in the phase-shift interferometry technique (Kreis 2005; Nomura *et al.* 2006). The field distribution of the stem cells at the detector plane (hologram plane) is represented as

$$O_{\mathrm{H}}(x,y) = A_{\mathrm{OH}}(x,y)\mathrm{e}^{j\phi_{\mathrm{OH}}(x,y)} = \iint_{d_0-\delta}^{d_0} \left\{ \frac{\mathrm{e}^{j2\pi z/\lambda}}{j\lambda z} \mathrm{e}^{j(\pi/\lambda z)(x^2+y^2)} O(\xi,\eta;z) \times \mathrm{e}^{j(\pi/\lambda z)(\xi^2+\eta^2)} \mathrm{e}^{-j(2\pi/\lambda z)(x\xi+y\eta)} \right\} \mathrm{d}z\,\mathrm{d}\xi\,\mathrm{d}\eta, \tag{2.1}$$

where $O(\xi,\eta;z)$ is the field distribution on the original stem cell surface at the reconstruction image plane (figure 2); d_0 is the distance between the centre of the focused stem cell at the image plane and the hologram plane; and δ is the cell's depth along the z-axis. Equation (2.1) represents the Fresnel transformation over a distance d_0, with object depth δ along the z-axis. The interference intensity pattern, i.e. the SEOL digital hologram between the diffracted wavefronts of the stem cell and the reference wave recorded at the image sensor array plane (hologram plane), is represented as follows:

$$H(x,y) = |A_{\mathrm{OH}}(x,y)|^2 + |A_{\mathrm{R}}|^2 + 2A_{\mathrm{OH}}(x,y)A_{\mathrm{R}}\cos[\phi_{\mathrm{OH}}(x,y) - \phi_{\mathrm{R}}], \tag{2.2}$$

where $A_{\mathrm{R}}\mathrm{e}^{j\phi_{\mathrm{R}}}$ is the reference wave at the hologram plane. The three-dimensional reconstruction of the original stem cell is performed computationally using the inverse Fresnel transformation of the SEOL digital hologram. Finally, the field distribution of the reconstructed three-dimensional stem cells from the SEOL digital hologram is represented as

$$\hat{O}(\xi,\eta) = \mathrm{IFT}(\mathrm{FT}\{H(x,y)\} \times \exp\left\{ j\pi\lambda d_0 \left[\frac{u^2}{(\Delta x N_x)^2} + \frac{v^2}{(\Delta y N_y)^2} \right] \right\}), \tag{2.3}$$

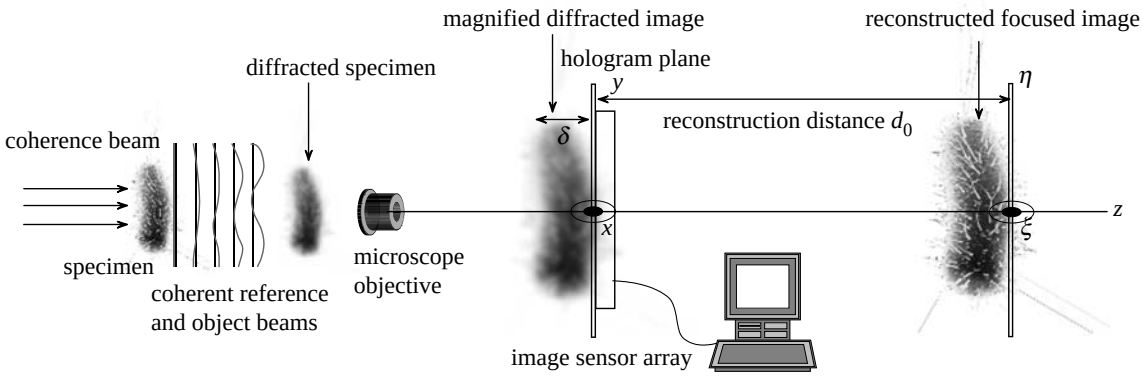

Figure 2. A schematic of the SEOL digital holography set-up for the three-dimensional sensing, recording and reconstruction of stem cells.

where d_0 is the distance between the hologram plane and the image plane, u and v denote the transverse discrete spatial frequencies, $(\Delta x, \Delta y)$ and (N_x, N_y) are the size and the number of pixels in the image sensor array at the hologram plane, respectively, and FT$\{\cdot\}$ denotes the Fourier transformation. In order to calculate the Fresnel diffraction integral, we use the angular spectrum method. The main difference between the angular spectrum method and the conventional Fresnel transform algorithm is that the angular spectrum method cancels the scale factor between the hologram plane and the object plane. Therefore, the transverse resolutions of the reconstruction plane are independent of a reconstruction distance in the longitudinal direction.

The reconstructed three-dimensional stem cell image from the SEOL digital hologram contains a conjugate image. This component generates an out-of-focus image that overlaps the reconstructed three-dimensional image of the stem cell. However, the defocused conjugate image also contains important information about the three-dimensional biological cells. As an additional merit, SEOL digital holography allows us to obtain a dynamic time-varying scene reconstructed digitally by the computer for monitoring and recognizing dividing and growing cells.

3. FEATURE EXTRACTION IN A DIGITAL HOLOGRAM OF STEM CELLS

In this section, we describe our use of the Gabor wavelet transformation (GWT) for extracting the feature vectors from a stem cell's interference pattern using SEOL digital holographic microscopy. GWT is very suitable for representing local feature vectors owing to the following useful properties: GWT is the best localized wavelet method; it provides the optimal compromise between spatial resolution and frequency resolution; and the Gabor kernel function has been successfully used for a number of image processing and two-dimensional object recognition applications (Lades *et al.* 1993; Lee 1996).

There are several benefits of using space–frequency analysis. First, the interference patterns often contain noisy fringe patterns created by the undesirable scattering of light off the surface of the optical components, which acts as noise in the recognition and identification of biological cells. GWT provides good noise tolerance due to the band-limited behaviour of the Gabor filters and the representation of the local features centred on feature points by the GWT coefficients. Therefore, the proposed three-dimensional recognition system is robust to the undesirable fringe patterns in the digital hologram and the DC components of the digital hologram can be removed. Second, one can extract the feature vectors from the SEOL digital hologram of stem cells. The separation between internal fringes varies with the width and thickness of the stem cell and the refractive index inside the stem cell. The Gabor wavelet transformation makes it possible to determine not only the global spatial frequency response of the interference fringes, but also the local features. Finally, the Gabor wavelet transformation makes it possible to separate the image over various spatial frequency components. We can obtain the local fringe pattern with the selected Gabor kernel function and successfully analyse the local interference patterns of the three-dimensional holographic image. The two-dimensional Gabor elementary function can be generalized as follows:

$$\begin{aligned}\psi(x, y) = \exp\{-[\alpha^2(x\cos\theta + y\sin\theta)^2 \\ + \beta^2(-x\sin\theta + y\cos\theta)^2]\} \\ \times \exp\{j2\pi f_0(x\cos\theta + y\sin\theta)\},\end{aligned} \tag{3.1}$$

where f_0 is the frequency of the sinusoid, θ is a rotation of the Gaussian and sinusoid functions, α is the sharpness of the Gaussian major axis and β is the sharpness of the Gaussian minor axis. The continuous wavelet transformation of the two-dimensional SEOL digital hologram $H(x,y)$ is defined by

$$\hat{H}(x, y) = H(x, y) * \psi(x, y), \tag{3.2}$$

where $(*)$ denotes convolution. Then, we computationally reconstruct the multi-scale and multi-resolution three-dimensional section images of the original stem cell at different depths along its longitudinal direction from each Gabor-filtered SEOL digital hologram using the inverse Fresnel transformation, which is as follows:

$$\hat{O}^S(\xi, \eta) = \mathrm{IFrT}[\hat{H}(x, y)]_{z=d_0 \text{ to } d_0+\delta}, \tag{3.3}$$

where IFrT$\{\cdot\}$ denotes the inverse Fresnel transformation.

4. THREE-DIMENSIONAL RECOGNITION OF STEM CELLS USING NON-PARAMETRIC STATISTICAL METHODS

In this section, we describe the statistical techniques for classification of stem cells. A statistical distribution-free test is employed for the comparison of two populations. Statistical sampling theory is useful in determining whether the observed differences between two samples are significant (Mukhopadhyay 2000). For the statistical decision, a hypothesis test can be performed by constructing the statistical sampling distribution of the test statistic. Let $X_1^S, \ldots, X_m^S$ denote the sample dataset, which is randomly selected from the Sth multi-scale image $\hat{O}^S$ (see equation (3.3)). For recognition and classification of stem cells, the ECDF can be obtained by the pixel values of the randomly selected m test pixels. Given m ordered data samples $X^s(1)$, $X^s(2)$, $X^s(3)$, ..., $X^s(m)$, the ECDF can be represented as

$$F(u) = \boldsymbol{P}(X^S(i) \le u) = \frac{\#\{X^S(i) \le u\}}{m}, \qquad (4.1)$$

where $X^s(\cdot)$ is the randomly selected pixel value in the Sth scaled image and $\#\{\mathrm{A}\}$ is the frequency of occurrence of the event A. The test statistics for the null hypothesis of a reference stem cell are defined by

$$\tilde{\Lambda} = \max\left\{|F_S^{\mathrm{ref}}(u) - \hat{F}_S^{\mathrm{ref}}(u)|\right\},$$
$$\tilde{D} = E\left\{\left[F_S^{\mathrm{ref}}(u) - \hat{F}_S^{\mathrm{ref}}(u)\right]^2\right\}, \qquad (4.2)$$

where $F_S^{\mathrm{ref}}(u)$ and $\hat{F}_S^{\mathrm{ref}}(u)$ are obtained from the Sth multi-scale image, generating n random data samples distributed according to $F_S^{\mathrm{ref}}(u)$, respectively. The possible values of $|F_S^{\mathrm{ref}}(u) - \hat{F}_S^{\mathrm{ref}}(u)|$ are in the range $0 \le |F_S^{\mathrm{ref}}(u) - \hat{F}_S^{\mathrm{ref}}(u)| \le 1$. In order to obtain the statistical sampling distribution of the test statistics, we actually form $\hat{F}_S^{\mathrm{ref}}(u)$ a number of times and then calculate the statistical distribution of $\tilde{\Lambda}$ and $\tilde{D}$ as the criterion discriminant function (CDF) appropriate for the null hypothesis. The test statistics for the input data are given by

$$\Lambda = \max\left\{|F_S^{\mathrm{ref}}(u) - F_S^{\mathrm{inp}}(u)|\right\},$$
$$D = E\left\{\left[F_S^{\mathrm{ref}}(u) - F_S^{\mathrm{inp}}(u)\right]^2\right\}. \qquad (4.3)$$

To perform the hypothesis testing, we set a null hypothesis H_0 and alterative hypothesis H_1 as follows:

$$H_0 : F_S^{\mathrm{ref}}(u) = F_S^{\mathrm{inp}}(u) \quad \text{for all } u, \quad \text{and}$$
$$H_1 : F_S^{\mathrm{ref}}(u) \ne F_S^{\mathrm{inp}} \quad \text{for at least one } u. \qquad (4.4)$$

Finally, we compute the statistical p-value, which is the probability that the variable with a probability density function $f\tilde{\Lambda}$ or $f\tilde{D}$ for the null hypothesis will be larger than the calculated statistics Λ or D for the statistical decision to classify the stem cells. The p-value is defined as (Mukhopadhyay 2000)

$$p\text{-value} = \int_{\Lambda}^{\infty} f\tilde{\Lambda}(t)\mathrm{d}t \quad \text{or} \quad \int_{D}^{\infty} f\tilde{D}(t)\mathrm{d}t, \qquad (4.5)$$

where $f\tilde{\Lambda}$ and $f\tilde{D}$ are the probability density functions for the statistics $\tilde{\Lambda}$ and $\tilde{D}$, respectively. Conventionally, the null hypothesis is rejected if the p-value is less than 0.05. However, other cut-off p-values are also applicable, for example 0.01 or 0.10.

5. EXPERIMENTAL RESULTS

We show the experimental results of three-dimensional image formation of three stem cells (*sunflower* and *corn* stem cells) using SEOL digital holographic microscopy, and three-dimensional recognition by optical coherent imaging in the Fresnel domain based on SEOL digital holographic microscopy using the non-parametric statistical methods and hypothesis testing.

5.1. *Visualization of three-dimensional stem cell images by SEOL digital holographic microscopy*

In this subsection, we present the visualization of typical plant stem cells by SEOL digital holographic microscopy. The SEOL digital hologram of the stem cells is recorded with an image sensor array of 2048×2048 pixels with a pixel size of 9×9 μm, where the specimen was sandwiched between two transparent cover-slips. For magnification of biological stem cells, we used a microscope objective with NA = 1.20 and a magnification of 60×. The transverse magnification of stem cells at the image plane is approximately $M_{\mathrm{t}} = 150\times$ and the reconstruction distance between the image plane and the hologram plane is approximately 200 mm. We calculate the magnified optical path difference (MOPD), $L_{\mathrm{OPD}} = M_{\mathrm{t}}^2 D|n_0 - n_{\mathrm{b}}| \approx 27$ mm to obtain the longitudinal volume depth information of the biological cells, where we assume that the thickness (D) of the plant stem cells is 12 μm, which is the typical thickness of plant stem cells. In addition, we assume the refractive index difference $|n_0 - n_b|$ between the stem cell and the surrounding medium to be 0.1. For three-dimensional volumetric imaging by SEOL digital holographic microscopy, we obtained the section images of the stem cells at an interval of approximately 0.5 μm between section images from 9 to 10.5 μm.

Figure 3*a–d* shows the sunflower stem cell three-dimensional image reconstructed at distances from 9 to 10.5 μm from the SEOL digital hologram, respectively. Figure 3*e,f* shows the sunflower and the corn stem cell three-dimensional images reconstructed at a distance of 9 μm from the SEOL digital hologram, respectively. The image in figure 3*a* was used as a reference, while the images in figure 3*e,f* were used as unknown input stem cells to test our recognition system.

5.2. *Feature-extracted three-dimensional images of stem cells using the Gabor wavelet method*

In this subsection, we show the process of reconstruction of three-dimensional images by Gabor wavelet filtering of the SEOL digital hologram of the stem cells. The Gabor wavelet filtering method is applied to enhance the discrimination capability between two

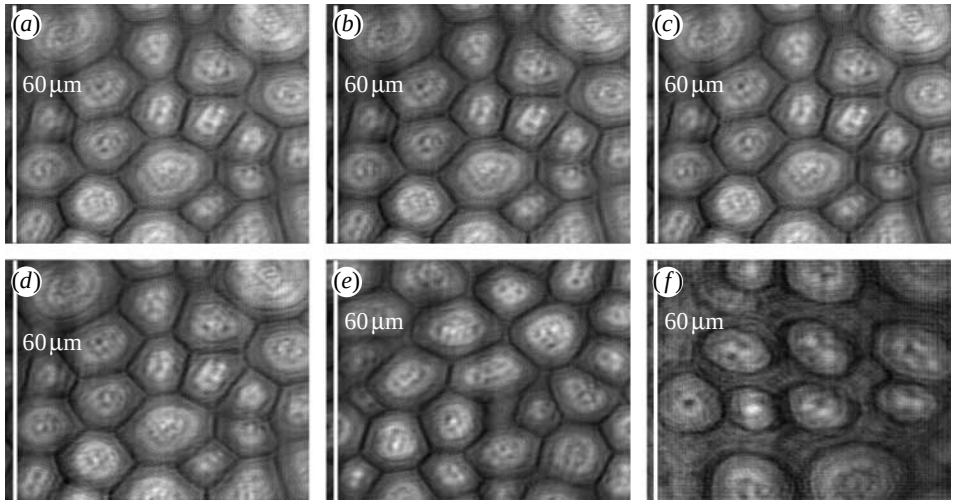

Figure 3. The sunflower stem cell three-dimensional images reconstructed at distances (*a*) 9, (*b*) 9.5, (*c*) 10 and (*d*) 10.5 μm. The image in (*a*) was used as a reference. The images in (*e*) and (*f*) were used as a true class (sunflower stem cell) and a false class (corn stem cell) input, respectively, and reconstructed at distance $d_0=9$ μm.

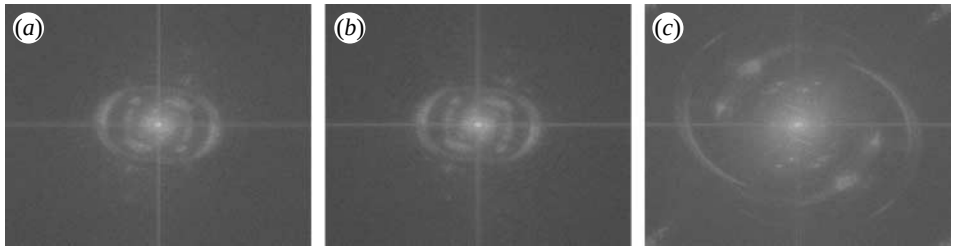

Figure 4. The Fourier spectrum of (*a*) the hologram of the sunflower stem cell (reference), (*b*) the hologram of the sunflower stem cell (true class input) and (*c*) the hologram of the corn stem cell (false class input).

datasets. The optimal kernel frequency of the Gabor wavelet function can be selected in such a way as to maximize the test statistic values defined in equation (4.3).

Fourier spectrum analysis for the digital holograms of stem cells has been performed. The results in figure 4 show that the digital holograms have a strong DC component and similar fringe patterns, which are generated by multiple reflections on various optical components due to the use of a coherent light source.

Figure 5 shows the sunflower stem cell three-dimensional images reconstructed by band-pass filtering of the SEOL digital hologram, where f_0 denotes the Gabor kernel frequency. In our experiment, we chose the carrier frequency of the band-pass filter in intervals of 0.005 from 0.01 to 0.50 and summed over all of the Gabor coefficients by changing the rotation angle of the Gabor kernel at intervals of 30° from 0 to 180° at each Gabor kernel frequency for the rotation-invariant property. α and β represent the sharpness of the Gaussian major and minor axes and are set to 2 and 1, respectively.

5.3. Non-parametric statistical method

In this subsection, we demonstrate a non-parametric statistical test to measure the similarity or dissimilarity between two datasets. We form the CDF for the two references, $F_S^{\mathrm{ref}}(u)$, from the real and the imaginary parts of the Sth multi-scale sunflower three-dimensional image reconstructed at the distance of 9 μm, where we randomly chose 5000 sample features from the reference image for fast processing. In order to obtain the statistical distribution of the test statistics for the null hypothesis, we form the two $\hat{F}_S^{\mathrm{ref}}(u)$ by selecting 500 random pixel points from the real and the imaginary parts of the Sth multi-scale reference image, respectively. We generated $\hat{F}_S^{\mathrm{ref}}(u)$ 100 times to obtain the statistical sampling distribution of the CDF $\tilde{D}$. Similarly, we construct the $F_S^{\mathrm{inp}}(u)$ by selecting 500 random pixel points from the real and the imaginary parts of the Sth multi-scaled unknown input image, where we generated $F_S^{\mathrm{inp}}(u)$ 100 times to obtain the statistical sampling distribution of the test statistic for the unknown input data.

Figure 6 shows the statistical distributions of $\tilde{D}$ as the CDF for the null hypothesis and the test statistic D for the true and the false classes, respectively, where the kernel frequency of the Gabor elementary function $k=0.30$ is used. In this experiment, we generated $\hat{F}_S^{\mathrm{ref}}(u)$ and $F_S^{\mathrm{inp}}(u)$ 100 times to construct the sampling distributions of the test statistic $\tilde{D}$ for the null hypothesis and the test statistic D for the input data, respectively. Then, we measured the central tendency of the statistical sampling distribution of the test statistic. Figure 6*c*,*d* shows the central tendency of each statistical sampling distribution from the two different input datasets. We see that the statistical sampling distributions of the test statistic D for the input datasets are totally different. It is noted that the three-dimensional

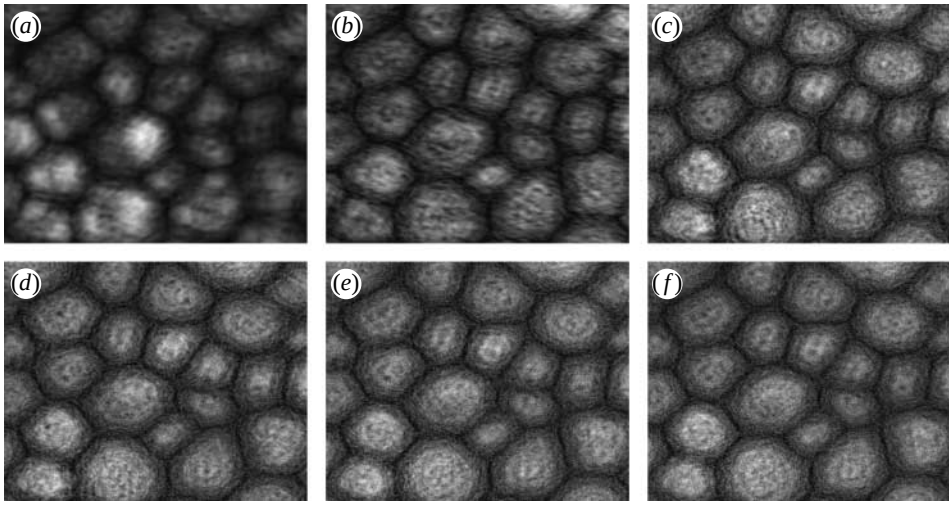

Figure 5. The feature-extracted sunflower stem cell three-dimensional images using the Gabor wavelet method, with (*a*) $f_0=0.1$, (*b*) $f_0=0.2$, (*c*) $f_0=0.3$, (*d*) $f_0=0.35$, (*e*) $f_0=0.40$ and (*f*) $f_0=0.45$.

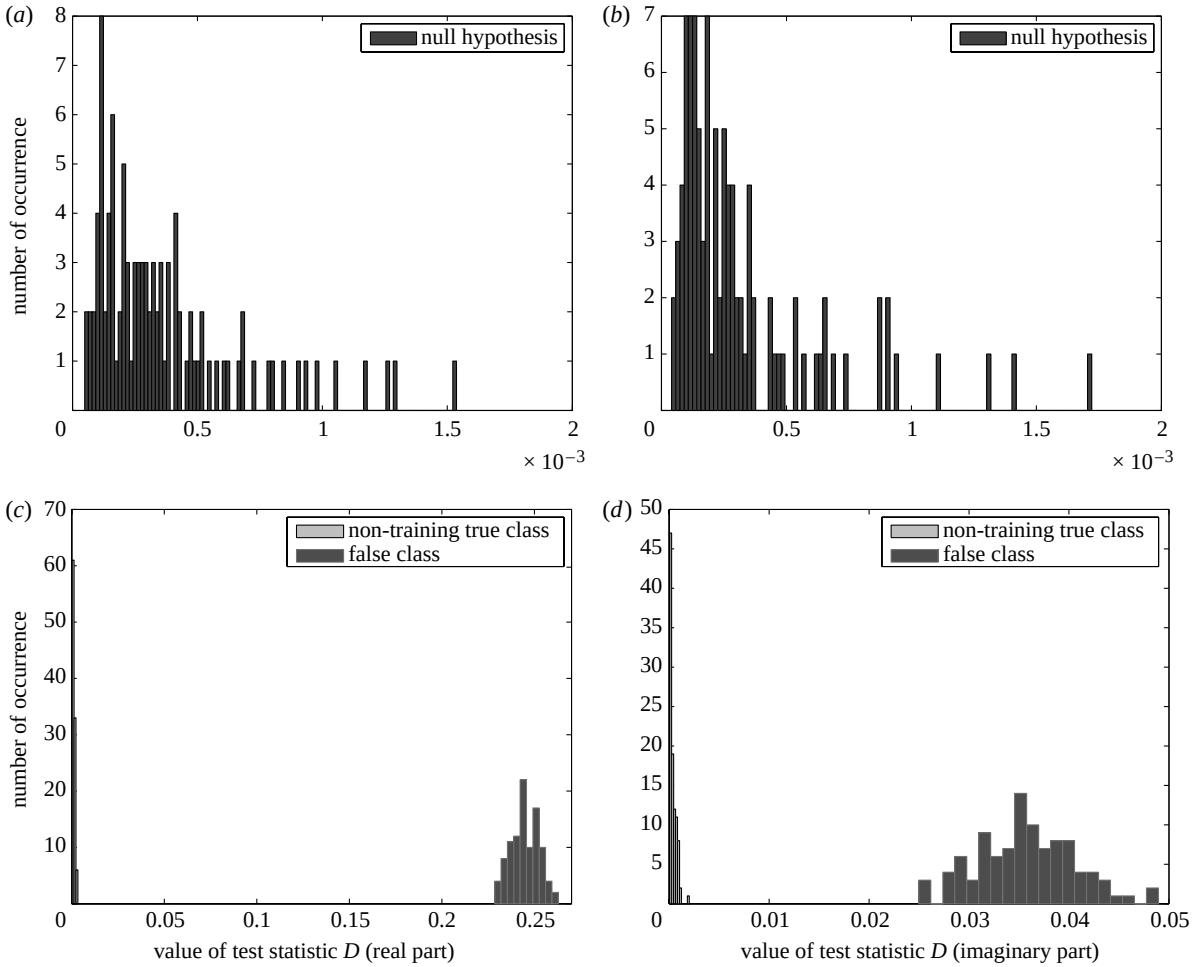

Figure 6. (*a*, *b*) The statistical sampling distributions of the test statistic $\tilde{D}$ for the null hypothesis. (*c*, *d*) The statistical sampling distributions of the test statistic D for the unknown input data. Null hypothesis is the true training class. Data are obtained from both the real and the imaginary parts in the multi-scale three-dimensional images.

image data obtained from the Gabor-filtered digital holograms of the stem cells have the distinguishing statistical distribution. As shown in figure 6, the maximum value of the CDF $\tilde{D}$ for the null hypothesis in the real and the imaginary parts are 0.0015 and 0.0017, respectively, and the mean values of the test statistic D in the real part for the true and false classes are 0.0012 and 0.2448, respectively. It is noted that every false class over 100 trial datasets was above the maximum value of the CDF $\tilde{D}$ for the null hypothesis.

To compare the value of the calculated test statistic using the unfiltered SEOL digital hologram, we also

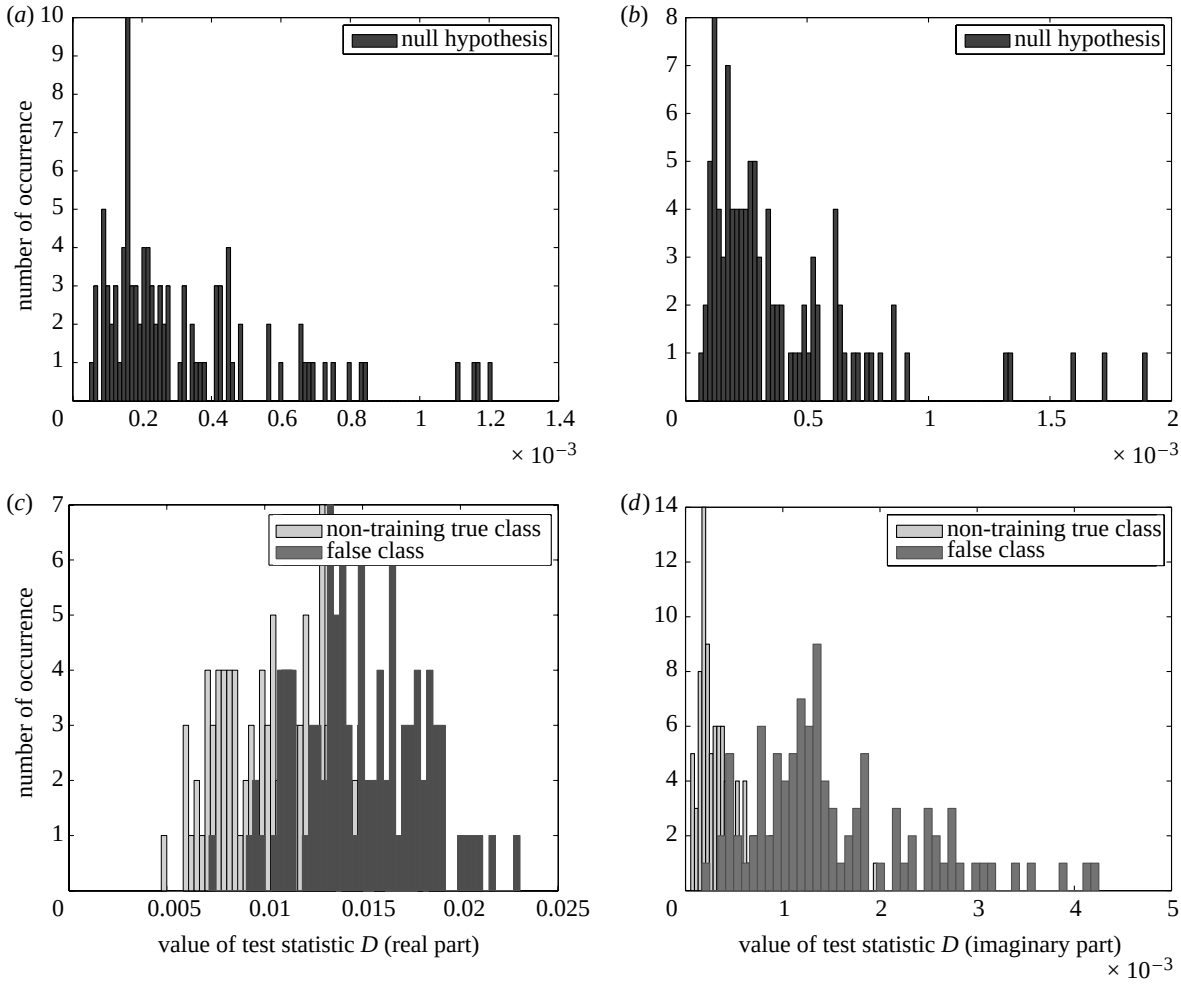

Figure 7. (*a*, *b*) The statistical sampling distributions of the test statistic for the null hypothesis. (*c*, *d*) The statistical sampling distributions of test statistic D for the unknown input data. Null hypothesis is the true training class. Data are obtained from the unfiltered SEOL digital hologram.

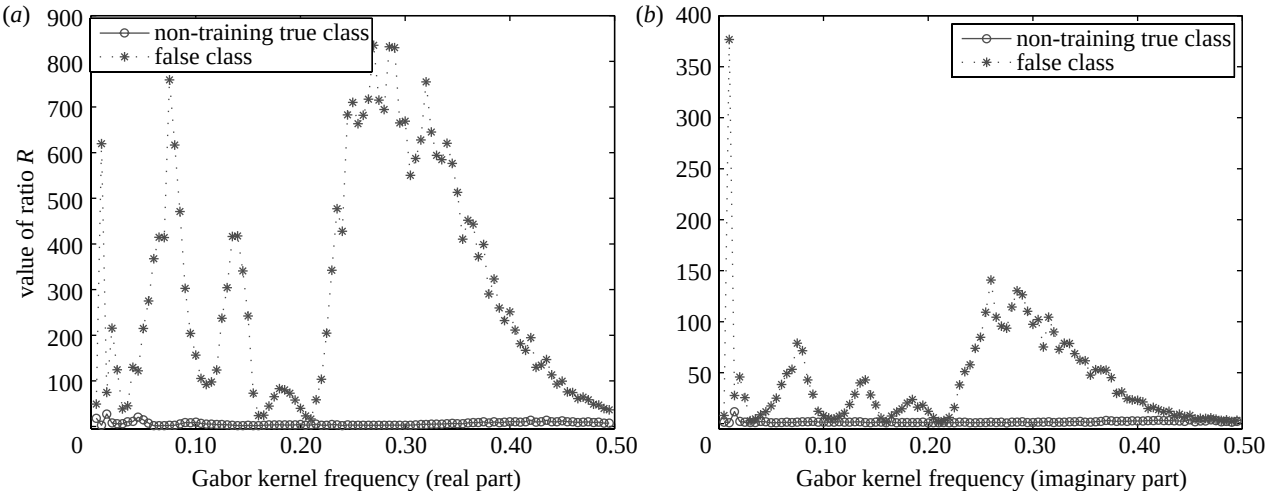

Figure 8. The experimental results show the values of the ratio R between the stem cells of the same class (true class) and different class (false class) using the multi-scale three-dimensional images; (*a*) real part and (*b*) imaginary part in the three-dimensional image.

compute the statistical distribution of the test statistic for the null hypothesis and unknown input data.

Figure 7 shows the statistical distributions of $\tilde{D}$ as the CDF for the null hypothesis and the test statistic D for the true and false classes, respectively. As shown in figure 7, the maximum value of the CDF $\tilde{D}$ for the null hypothesis in the real and the imaginary parts are 0.0012 and 0.0019, respectively, and the mean values of

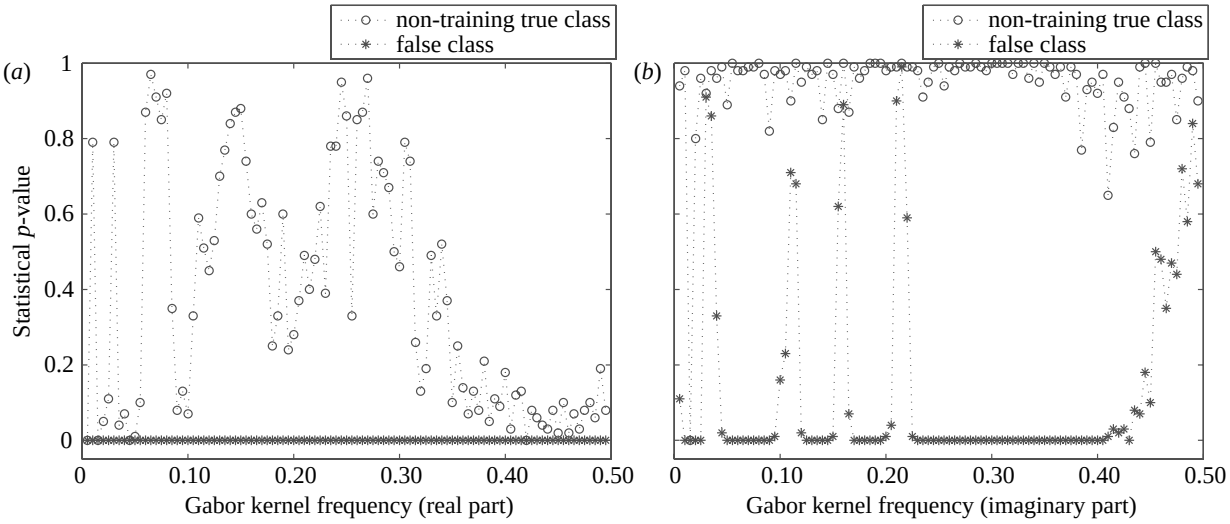

Figure 9. The experimental results show the statistical p-values between the stem cells of the same class (true class) and different class (false class) using the multi-scale three-dimensional images; (a) real part and (b) imaginary part in the three-dimensional image.

the test statistic D in the real part for the true and false classes are 0.0106 and 0.0150, respectively. It is noted that the mean values of the true and the false classes over 100 trial datasets were above the maximum value of the CDF $\tilde{D}$ for the null hypothesis. In this case, it is difficult to measure the similarity or dissimilarity between two datasets by the unfiltered SEOL digital hologram.

To evaluate the performance of our three-dimensional recognition system, we define the following ratio between the null hypothesis for the true class and unknown input data:

$$R = \frac{\text{averaged test statistic 's value for the unknown input data}}{\text{averaged test statistic 's value for the null hypothesis}}.$$

In order to select an optimal kernel frequency to maximize the ratio R, we calculate R while changing the kernel frequency of the Gabor elementary function at intervals of 0.005 from 0.010 to 0.500. Figure 8 shows the experimental results of the calculated ratio R. As shown in figure 8, most of the values of R for the non-training true class in the real and the imaginary parts are close to 1, while most of the values of R for the false classes are greater than 10. It is noted that the optimal Gabor kernel frequency to maximize the discrimination between two stem cells are 0.275 and 0.015 in the real and the imaginary parts, respectively.

We also compute the statistical p-value defined in equation (4.5) and we conduct the hypothesis testing with the calculated p-value for the statistical decision to classify the stem cells. Figure 9 shows the calculated statistical p-value, where the minimum value of the test statistic D over 100 trial datasets was selected. As shown in figure 9, most of the p-values for the non-training true class were greater than 0.01 in the real and the imaginary parts, while most of the p-values for the false class were less than 0.01 in the real and the imaginary parts. We can reject the null hypothesis, H_0, defined in equation (4.4) in the case where the value of the test statistic is larger than the value of the CDF $\tilde{D}$ at a level of significance of 0.01. It is noted that the percentages of correctly matched sample data over 100 trial datasets in the real part for the true class are approximately 100% by the decision rule, while for the false class the percentages are approximately 0%. These experimental results indicate that there is a considerable similarity in the range of the Gabor kernel frequency ($0.15 < f_0 < 0.35$) between the reference and the true class input. Thus, preliminary experimental results indicate that it may be possible to classify stem cells using the multi-scale three-dimensional images obtained by the Gabor-based band-pass-filtered SEOL digital hologram and the non-parametric statistical method.

6. CONCLUSION

In conclusion, we have presented a three-dimensional sensing and recognition system of stem cells using SEOL digital holographic microscopy, Gabor wavelet analysis, and non-parametric statistical estimation and inference algorithms. We optically obtained the Fresnel diffraction intensity patterns of stem cells by the use of SEOL digital holographic microscopy. For feature extraction and removal of DC components from the SEOL digital hologram, we computationally extracted the local feature vectors from the Fresnel-diffracted holograms of the stem cells using the Gabor wavelet transformation. Then, we digitally reconstructed the three-dimensional focused images from the Gabor-filtered SEOL digital hologram. For three-dimensional recognition, the test pixel points are randomly selected from the multi-scale three-dimensional image. Then, the ECDF is formed by the test pixel values according to the proposed design procedure. For statistical decision on the basis of the statistical sampling distribution of the datasets, the hypothesis testing for the equality between the CDFs of two populations has been performed.

We have presented the experimental results for three-dimensional recognition and classification of stem cells adopting the statistical method and inference algorithms. It has been shown in experiments that we can successfully classify stem cells and the recognition capacity is considerably increased by using the Gabor

wavelet-filtered SEOL digital hologram, with the results compared with those from an unfiltered SEOL digital hologram. The optimal Gabor kernel frequency, which increases the discrimination performance, is selected using the multi-scale three-dimensional images.

This work has been supported in part by the Defense Advanced Research Projects Agency (DARPA). The authors are grateful to the anonymous reviewers for their valuable comments and suggestions.

REFERENCES

Daugman, J. G. 1985 Uncertainty relation for resolution in space, spatial frequency, and orientation optimized by two-dimensional visual cortical filters. *J. Opt. Soc. Am.* **2**, 1160–1169.

Frauel, Y. & Javidi, B. 2001 Neural network for three-dimensional object recognition based on digital holography. *Opt. Lett.* **26**, 1478–1480.

Gabor, D. 1946 Theory of communication. *J. Inst. Elect. Eng.* **93**, 429–459.

Goodman, J. W. & Lawrence, R. W. 1967 Digital image formation from electronically detected holograms. *Appl. Phys. Lett.* **11**, 77–79. (doi:10.1063/1.1755043)

Hollander, M. & Wolfe, D. A. 1999 *Nonparametric statistical methods*. New York, NY: Wiley.

Javidi, B. (ed.) 2002 *Image recognition and classification: algorithms, systems, and applications*. New York, NY: Marcel Dekker.

Javidi, B. & Kim, D. 2005 Three-dimensional-object recognition by use of single-exposure on-axis digital holography. *Opt. Lett.* **30**, 236–238. (doi:10.1364/OL.30.000236)

Javidi, B. & Tajahuerce, E. 2000 Three dimensional object recognition using digital holography. *Opt. Lett.* **25**, 610–612.

Javidi, B., Moon, I., Yeom, S. & Carapezza, E. 2005 Three-dimensional imaging and recognition of microorganism using single-exposure on-line (SEOL) digital holography. *Opt. Exp.* **13**, 4492–4506. (doi:10.1364/OPEX.13.004492)

Kreis, T. (ed.) 2005 *Handbook of holographic interferometry*. New York, NY: Wiley-VCH.

Lades, M., Vorbruggen, J. C., Buhmann, J., Lange, J., von der Malsburg, C., Wurtz, R. P. & Konen, W. 1993 Distortion invariant object recognition in the dynamic link architecture. *IEEE Trans. Comput.* **42**, 300–311. (doi:10.1109/12.210173)

Lee, T. S. 1996 Image representation using 2D Gabor wavelets. *IEEE Trans. Pattern Anal. Machine Intell.* **18**, 959–971. (doi:10.1109/34.506415)

Moon, I. & Javidi, B. 2005 Shape-tolerant three-dimensional recognition of microorganisms using digital holography. *Opt. Exp.* **13**, 9612–9622. (doi:10.1364/OPEX.13.009612)

Moon, I. & Javidi, B. In press. Volumetric 3D recognition of biological microorganisms using multivariate statistical method and digital holography. *J. Biomed. Opt.*

Mukhopadhyay, N. (ed.) 2000 *Probability and statistical inference*. New York, NY: Marcel Dekker.

National Institutes of Health 2004 *Stem cells: scientific progress and future research directions*. Park Forest, IL: University Press of the Pacific.

Nomura, T., Murata, S., Nitanai, E. & Numata, T. 2006 Phase-shifting digital holography with a phase difference between orthogonal polarizations. *Appl. Opt.* **45**, 4873–4877. (doi:10.1364/AO.45.004873)

Oppenheim, A., Willsky, A., Hamid, S. & Nawab, S. 1996 *Signals and systems*. Englewood Cliffs, NJ: Prentice Hall.

Osten, W., Baumbach, T. & Jüptner, W. 2002 Comparative digital holography. *Opt. Lett.* **27**, 1764–1766.

Shortt, A. E., Naughton, T. J. & Javidi, B. 2006 Compression of digital holograms of three-dimensional objects using wavelets. *Opt. Exp.* **14**, 2625–2630. (doi:10.1364/OE.14.002625)

Shostak, S. 2006 (Re)defining stem cells. *Bioessays* **28**, 301–308. (doi:10.1002/bies.20376)

Tajahuerce, E., Matoba, O. & Javidi, B. 2001 Shift-invariant three-dimensional object recognition by means of digital holography. *Appl. Opt.* **40**, 3877–3886.

Yatagai, T., Ohmura, K., Iwasaki, S., Hasegawa, S., Endo, J. & Tonomura, A. 1987 Quantitative phase analysis in electron holographic interferometry. *Appl. Opt.* **26**, 377–382.